

Hydrodynamic correlation functions of a driven granular fluid in steady stateKatharina Vollmayr-Lee,^{1,*} Timo Aspelmeier,^{2,3} and Annette Zippelius^{2,4}¹*Department of Physics and Astronomy, Bucknell University, Lewisburg, Pennsylvania 17837, USA*²*Max-Planck-Institut für Dynamik und Selbstorganisation, Bunsenstr. 10, D-37073 Göttingen, Germany*³*Scivis GmbH, Bertha-von-Suttner-Str. 5, D-37085 Göttingen, Germany*⁴*Georg-August-Universität Göttingen, Institut für Theoretische Physik, Friedrich-Hund-Platz 1, D-37077 Göttingen, Germany*

(Received 28 July 2010; revised manuscript received 5 November 2010; published 5 January 2011)

We study a homogeneously driven granular fluid of hard spheres at intermediate volume fractions and focus on time-delayed correlation functions in the stationary state. Inelastic collisions are modeled by incomplete normal restitution, allowing for efficient simulations with an event-driven algorithm. The incoherent scattering function $F_{\text{incoh}}(q, t)$ is seen to follow time-density superposition with a relaxation time that increases significantly as the volume fraction increases. The statistics of particle displacements is approximately Gaussian. For the coherent scattering function $S(q, \omega)$, we compare our results to the predictions of generalized fluctuating hydrodynamics, which takes into account that temperature fluctuations decay either diffusively or with a finite relaxation rate, depending on wave number and inelasticity. For sufficiently small wave number q we observe sound waves in the coherent scattering function $S(q, \omega)$ and the longitudinal current correlation function $C_1(q, \omega)$. We determine the speed of sound and the transport coefficients and compare them to the results of kinetic theory.

DOI: [10.1103/PhysRevE.83.011301](https://doi.org/10.1103/PhysRevE.83.011301)

PACS number(s): 45.70.-n, 61.20.Lc, 51.20.+d, 47.57.Gc

I. INTRODUCTION

The long-wavelength, low-frequency dynamics of granular fluids is frequently described by phenomenological hydrodynamic equations [1–4]. In contrast to a fluid composed of elastically colliding particles, the total energy of the system is not conserved, implying a finite decay rate of the temperature in the limit of long wavelength. Hence, strictly speaking, the temperature is not a hydrodynamic variable. More generally, the scale separation required by hydrodynamics has been questioned [5]. If the system is not driven, the homogeneous state is unstable [6] and large spatial gradients develop—invalidating a hydrodynamic approach for asymptotically long times. A third point of criticism refers to the pressure in the Navier-Stokes equation. Closure of the hydrodynamic equations requires an equation of state to express the pressure [7] in terms of density and temperature. However, an equation of state is expected to exist only in an equilibrium state. Given these problems, the hydrodynamic approach has been restricted mainly to small inelasticity, such that the decay rate of the temperature is low, the time for the buildup of spatial inhomogeneities is long, and an equation of state is approximately valid. In this limit, kinetic theory has provided a basis for the hydrodynamic equations and given explicit expressions for the transport coefficients [8–10].

Driving a granular fluid allows for compensation of the energy that is dissipated in collisions, such that a nonequilibrium stationary state (NESS) is reached. In experiment, the driving is frequently performed by shearing [11,12], with vibrating walls [13–15] or by driving the system homogeneously [16,17]. To test a hydrodynamic approach in the NESS we want to avoid new length scales, which might be generated by driving through the boundaries, when the agitation decays over a

characteristic length, e.g., the width of a shear band. Hence, in the following, we consider a homogeneously driven granular fluid [18–22] and set out to investigate the validity of the hydrodynamic approach in the NESS.

In this paper we present results for a homogeneously driven system of hard spheres with moderate inelasticity, parametrized by a coefficient of restitution $\epsilon = 0.8, 0.9$, and 1.0 (elastic). We use event-driven simulations to focus on the dynamics of the system. Previous studies of correlation functions for granular fluids have been either on density-density correlations at the same time, such as the structure factor $S(q)$ [18,19] and the pair correlation function [23], or on velocity-velocity correlations [[21], and references therein]. We focus here on time-dependent spatial correlations [22] at volume fraction $0.05 \leq \eta \leq 0.4$ and compute the incoherent and coherent intermediate scattering functions.

The former entails information about the motion of a tagged particle, which is expected to be diffusive at long times. We find that the incoherent scattering function is well approximated by a Gaussian and obeys time-density superposition. The divergence of the relaxation time as a function of η occurs not only for the elastic case but also for the inelastic case, consistent with the results of Reyes *et al.* [14,22].

The coherent correlations reveal the collective dynamics of the fluid: damped sound waves and relaxation of temperature fluctuations. We determine the dynamic structure factor $S(q, \omega)$ and compare our data quantitatively to the predictions of van Noije *et al.* [19] using fluctuating hydrodynamics. The agreement between simulations and theory is quite good: damped sound waves are indeed observed for small wave numbers q and the velocity and damping of sound can be determined. Temperature fluctuations are found to decay either diffusively or at a finite rate, depending on q . The transport coefficients are compared to the predictions of kinetic theory and found to agree well.

In the following, we specify model and simulation details in Sec. II. Then, in Sec. III, we discuss the incoherent scattering

*Author to whom correspondence should be addressed.
kvollmayr@bucknell.edu

function, the mean square displacement, and the diffusion constant. Data on the intermediate coherent scattering function and longitudinal current correlation function are presented in Sec. IV. A hydrodynamic model, which was first introduced in Ref. [18], is discussed in Sec. V and compared to the simulation data for the coherent scattering function in Sec. VI.

II. MODEL AND SIMULATION DETAILS

We investigate a system of N monodisperse hard spheres of diameter a and mass m at volume fraction $\eta = \frac{N\pi a^3}{6V}$. The time evolution is governed by instantaneous inelastic two-particle collisions. We consider here only the simplest model of an inelastic two-body collision, described by incomplete normal restitution. The change in the relative velocity $\mathbf{g} := \mathbf{v}_1 - \mathbf{v}_2$ of the two colliding particles is given by

$$(\mathbf{g} \cdot \mathbf{n})' = -\varepsilon(\mathbf{g} \cdot \mathbf{n}), \quad (1)$$

where primed quantities indicate postcollisional velocities and unprimed ones refer to precollisional ones. The unit vector $\mathbf{n} := (\mathbf{r}_1 - \mathbf{r}_2)/|\mathbf{r}_1 - \mathbf{r}_2|$ connects the centers of the two spheres, and $\varepsilon = \text{const.} \in [0, 1]$ denotes the coefficient of normal restitution, with $\varepsilon = 1.0$ in the elastic limit. The postcollisional velocities of the two colliding spheres are given by

$$\mathbf{v}'_1 = \mathbf{v}_1 - \frac{(1 + \varepsilon)}{2}(\mathbf{n} \cdot \mathbf{g})\mathbf{n}, \quad (2)$$

$$\mathbf{v}'_2 = \mathbf{v}_2 + \frac{(1 + \varepsilon)}{2}(\mathbf{n} \cdot \mathbf{g})\mathbf{n}. \quad (3)$$

Due to the inelastic nature of the collisions, we have to feed energy into the system to maintain a stationary state. The simplest bulk driving [24] consists of a kick of a given particle, say particle i , instantaneously at time t , which corresponds to

$$\mathbf{v}_i(t) = \mathbf{v}_i(t_0) + \int_{t_0}^t ds \xi_i(s). \quad (4)$$

The noise $\xi_i(t)$ is Gaussian with zero mean and variance,

$$\langle \xi_i^{(\alpha)}(t) \xi_j^{(\beta)}(t') \rangle = \xi_0^2 \delta_{i,j} \delta_{\alpha\beta} \delta(t - t'), \quad (5)$$

for the Cartesian components $\xi_i^{(\alpha)}$, $\alpha = x, y, z$. The stochastic process is implemented in the simulation by kicking the particles randomly with amplitude v_{Dr} and frequency f_{Dr} .

If a single particle is kicked at a particular instant, momentum is not conserved. Due to the random direction of the kicks, the time average will restore the conservation of global momentum, but only on average. Momentum conservation is known to be essential for the dynamic correlation functions in the limit of long wavelength and long times. Hence we choose a driving mechanism in which pairs of particles are kicked in opposite directions [25]. The pairs are fixed globally so that the total momentum is conserved at each instant of time. Denoting the partner of particle i by $p(i)$, the random force correlation is given by

$$\langle \xi_i^{(\alpha)}(t) \xi_j^{(\beta)}(t') \rangle = \xi_0^2 (\delta_{j,i} - \delta_{j,p(i)}) \delta_{\alpha\beta} \delta(t - t'). \quad (6)$$

It is also possible to ensure momentum conservation on small scales by choosing pairs of neighboring particles and by

kicking them in opposite directions. However, this is not pursued here.

For the event-driven simulations we use the optimized algorithm of Lubachevsky [26] adapted to granular media [21]. To avoid the inelastic collapse we use the technique of virtual hulls around the spheres as described in Ref. [21]. Particles are colliding elastically when they are a diameter a apart, and dissipation takes place when the colliding spheres are receding and separated by $(1 + 10^{-4})a$.

With the appropriate choice of $v_{\text{Dr}}^2 f_{\text{Dr}} = \xi_0^2$, we ensured constant temperature, and throughout the following we chose units such that $m = a = T = 1$. All simulations were with a cubic box and periodic boundary conditions. The simulation results in Sec. III are for $N = 200,000$ and two independent simulation runs,¹ whereas for the results in Secs. IV and VI we needed more statistics and therefore used $N = 10,000$ and 100 independent simulation runs, respectively. In each set of simulations we first equilibrated at $\varepsilon = 1.0$ at the desired volume fraction; this was followed by a relaxation to a stationary state at $\varepsilon \neq 1$ (achieved with a simulation run of at least 100 time units) and consecutive production runs. Independent configurations were taken from the initial elastic equilibration run separated in time by at least 1000 time units.

III. INTERMEDIATE INCOHERENT SCATTERING FUNCTION AND SELF-DIFFUSION CONSTANT

In this section we investigate time-delayed correlations of a single tagged particle. In Fig. 1 we show, for volume fractions $0.05 \leq \eta \leq 0.4$ and for inelasticities $\varepsilon = 0.8, 0.9$, and 1.0 the

¹The only exception is the results in Fig. 4, for which we used five independent simulation runs.

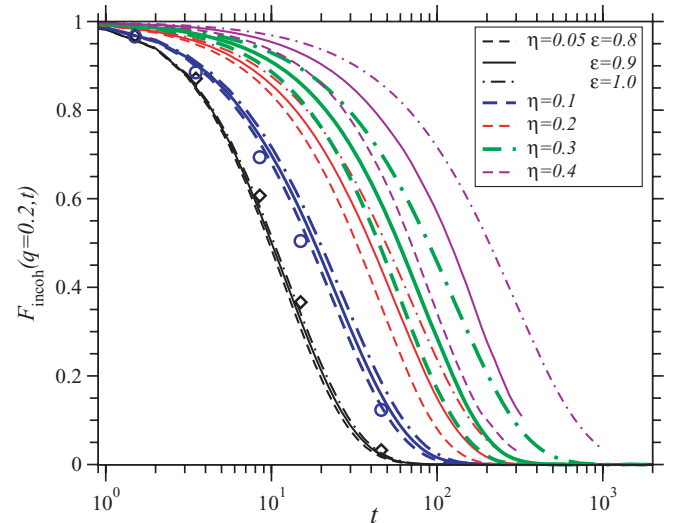


FIG. 1. (Color online) Incoherent intermediate scattering function for several values of volume fraction η and coefficient of restitution ε . All lines for $N = 200,000$, where $\varepsilon = 0.8, 0.9$, and 1.0 , are indicated by dashed, solid, and dot-dashed lines, respectively. $\eta = 0.05$ corresponds to the left, and $\eta = 0.4$ to the right, lines. All error bars are of the order 10^{-3} . Open diamonds and circles are for $N = 10,000$, $\varepsilon = 0.8$, and $\eta = 0.05$ and 0.1 , respectively.

incoherent intermediate scattering function,

$$F_{\text{incoh}}(\mathbf{q}, t) = \left\langle \frac{1}{N} \sum_{i=1}^N e^{i\mathbf{q} \cdot [\mathbf{r}_i(t) - \mathbf{r}_i(0)]} \right\rangle. \quad (7)$$

Here the average $\langle \dots \rangle$ is performed over initial conditions and the noise, Eq. (6).

Since $F_{\text{incoh}}(\mathbf{q}, t)$ is a measure of the correlation of particle i at position $\mathbf{r}_i(t)$ at time t and at position $\mathbf{r}_i(0)$ at time $t = 0$, we find, as expected, that $F_{\text{incoh}}(\mathbf{q}, t)$ decreases with increasing time. With decreasing densities the $\mathbf{r}_i(t)$ and $\mathbf{r}_i(0)$ become more quickly uncorrelated and therefore the decay is faster for smaller volume fractions. For the lowest densities the inelastic system can hardly be distinguished from the elastic case. For higher densities the relaxation is increasingly faster for the more inelastic systems, presumably because the more inelastic systems need stronger driving to achieve comparable temperatures. To quantify this effect, in Fig. 2 we plot the relaxation time τ when the incoherent intermediate scattering function has decayed to $1/e$ of its initial value, that is, $F_{\text{incoh}}(\mathbf{q}, \tau) = 1/e$. Clearly the elastic system shows the most rapid increase in relaxation time with density, even though the highest volume fraction ($\eta = 0.4$) is still well below the critical value for the glass transition. The slowing-down is weaker for inelastic systems. However, the inelastic system also shows an increase by a factor of 12 ($\varepsilon = 0.9$) and 7 ($\varepsilon = 0.8$). This indication of a precursor of a glass transition even for the inelastic system is consistent with the higher density results of Kranz *et al.* [22] (theory and simulation) and of Reis *et al.* [27] and Reyes *et al.* [14] (experiment).

The intermediate incoherent scattering function $F_{\text{incoh}}(\mathbf{q}, t)$ is often approximated by a Gaussian,

$$F_{\text{incoh}}(\mathbf{q}, t) = e^{-\frac{q^2}{6} \langle \Delta r^2(t) \rangle}, \quad (8)$$

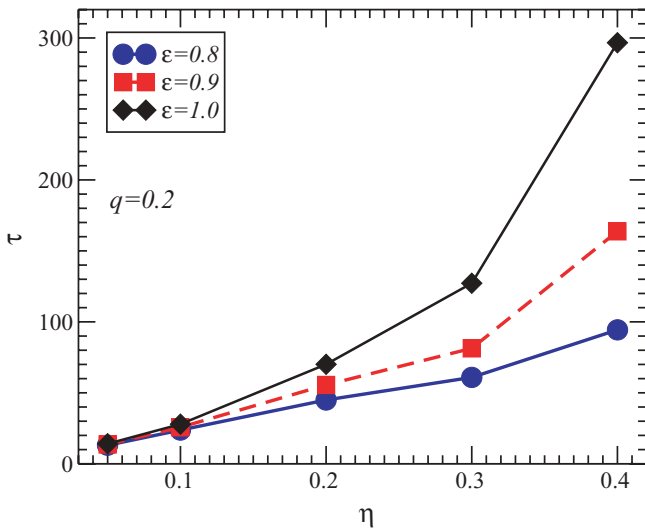


FIG. 2. (Color online) Relaxation time of the incoherent scattering function as a function of volume fraction η for several values of ε for simulation runs with $N = 200,000$ particles.

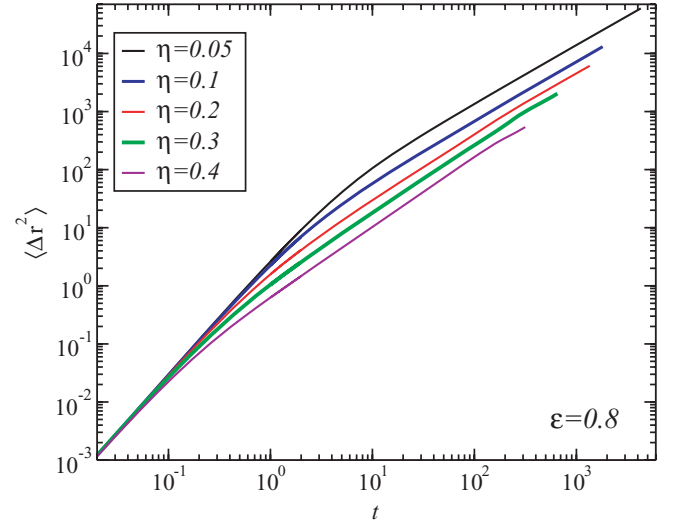


FIG. 3. (Color online) Mean square displacement for $\varepsilon = 0.8$ and various volume fractions, ranging from $\eta = 0.05$ [top (black) line] to $\eta = 0.4$ [bottom (violet) line].

with mean square displacement

$$\langle \Delta r^2(t) \rangle = \left\langle \frac{1}{N} \sum_{i=1}^N (\mathbf{r}_i(t) - \mathbf{r}_i(0))^2 \right\rangle, \quad (9)$$

assuming that $\Delta \mathbf{r} = (\mathbf{r}_i(t) - \mathbf{r}_i(0))$ obeys Gaussian statistics. To test this hypothesis we first compute the mean square displacement $\langle \Delta r^2(t) \rangle$. Figure 3 shows the resulting $\langle \Delta r^2(t) \rangle$ for $\varepsilon = 0.8$ and several volume fractions. One clearly observes a ballistic regime for small times, with a crossover to diffusive behavior around $t \sim 1$.

The computed $\langle \Delta r^2(t) \rangle$ is then substituted in the Gaussian approximation of Eq. (8) and compared to the full scattering function in Fig. 4. The Gaussian approximation works very well for the densities under consideration.

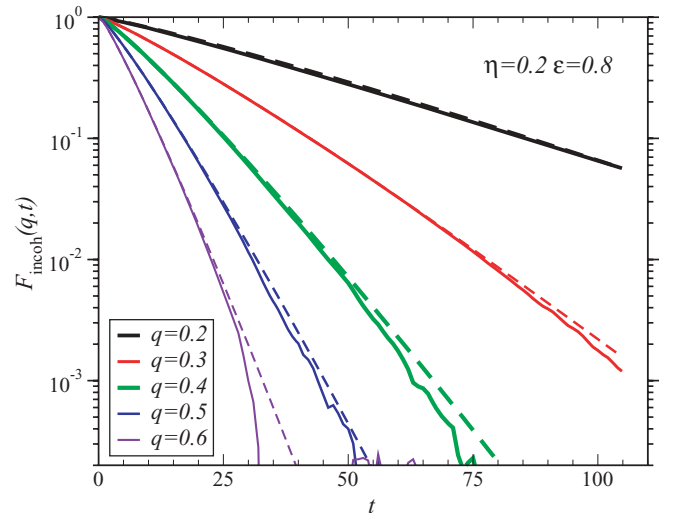


FIG. 4. (Color online) Intermediate incoherent scattering function $F_{\text{incoh}}(\mathbf{q}, t)$ using Eq. (7) (solid lines) and, for comparison, the Gaussian approximation using Eqs. (8) and (9) (dashed lines).

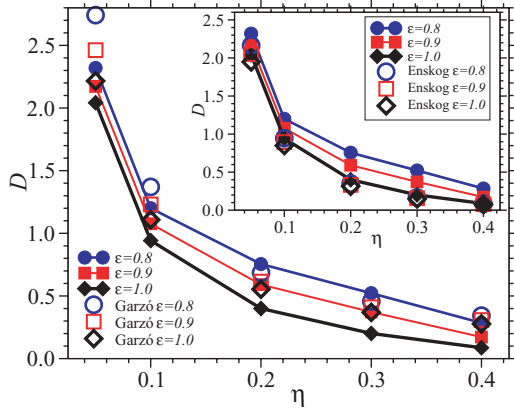


FIG. 5. (Color online) Self-diffusion constant D as a function of volume fraction η . Filled symbols, with lines to guide the eye, were obtained via linear fits to the mean square displacement for large times. Garzó results correspond to Eq. (2.10) of Ref. [28], and the Enskog result corresponds to Eq. (5) of Ref. [21].

We can also extract the self-diffusion coefficient,

$$D = \lim_{t \rightarrow \infty} \frac{\langle \Delta r^2(t) \rangle}{6t}, \quad (10)$$

via a linear fit to $\langle \Delta r^2(t) \rangle$ at long times. The resulting D is plotted in Fig. 5 as a function of density (filled symbols) and compared with theoretical predictions (open symbols). As expected, the diffusion constant decreases strongly with the density. Whereas the prediction of Enskog (see Eq. (5) of Ref. [21]) is in excellent agreement for the elastic case (see inset), the prediction of Garzó [28] is very good for the inelastic case and $\eta > 0.1$.

For the glass transition in elastic systems, one observes dynamic scaling as the transition is approached. In other words, the scattering function does not depend separately on time and the control parameter—either temperature or density—but only on the ratio t/τ . We have tested this time-density superposition principle by plotting $F_{\text{incoh}}(\mathbf{q}, t/\tau)$ for five volume fractions in Fig. 6. Even though the volume

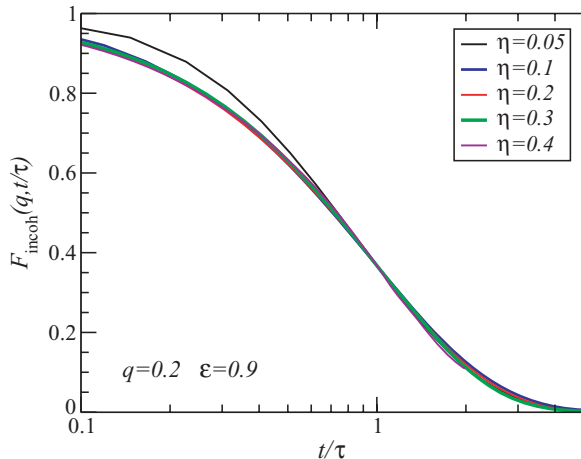


FIG. 6. (Color online) Time-density superposition for the incoherent scattering function.

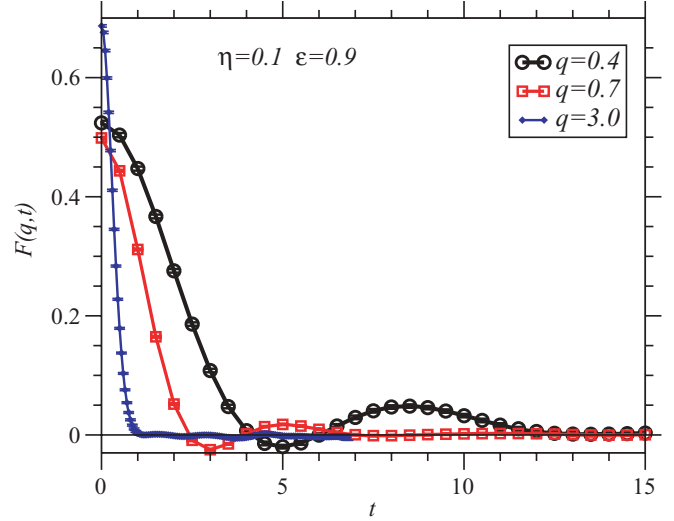


FIG. 7. (Color online) Intermediate coherent scattering function $F(q, t)$.

fractions under consideration are far away from the critical value, the data collapse for $\eta \geq 0.1$.

IV. INTERMEDIATE COHERENT SCATTERING FUNCTION AND LONGITUDINAL CURRENT CORRELATION

Information about the collective dynamics and, in particular, the collective density fluctuations is contained in the intermediate *coherent* scattering function, defined by

$$F(\mathbf{q}, t) = \left\langle \frac{1}{N} \sum_{i,j=1}^N e^{i\mathbf{q} \cdot [\mathbf{r}_i(t) - \mathbf{r}_j(0)]} \right\rangle. \quad (11)$$

In the hydrodynamic regime, that is, small wave numbers, we expect to see sound modes. This expectation is indeed borne out by the data, with an example shown in Fig. 7 for volume fraction $\eta = 0.1$, restitution coefficient $\epsilon = 0.9$, and several q values. We observe oscillations that are overdamped for large q . A detailed analysis of the coherent correlation in terms of damped sound waves and temperature fluctuations is given in Sec. VI, using a hydrodynamic model discussed in the next section. Here we consider the longitudinal current correlation to obtain an approximation of the sound velocity, which we analyze in dependence on volume fraction and inelasticity. The correlation of the longitudinal current is defined as

$$\begin{aligned} C_l(\mathbf{q}, t) &= \left\langle \frac{1}{N} \sum_{i,j=1}^N \frac{1}{q^2} (\mathbf{q} \cdot \mathbf{v}_i)(\mathbf{q} \cdot \mathbf{v}_j) e^{i\mathbf{q} \cdot [\mathbf{r}_i(t) - \mathbf{r}_j(0)]} \right\rangle \\ &= -\frac{1}{q^2} \partial_t^2 F(\mathbf{q}, t). \end{aligned} \quad (12)$$

In Fig. 8 we show data for two values of restitution and volume fractions $0.05 \leq \eta \leq 0.2$. For all parameters we observe well-defined oscillations, which are more strongly damped for more inelastic systems.

In Fig. 9 we plot $C_l(\mathbf{q}, \omega)$, the corresponding Fourier transform of the current correlation. A rough estimate of the

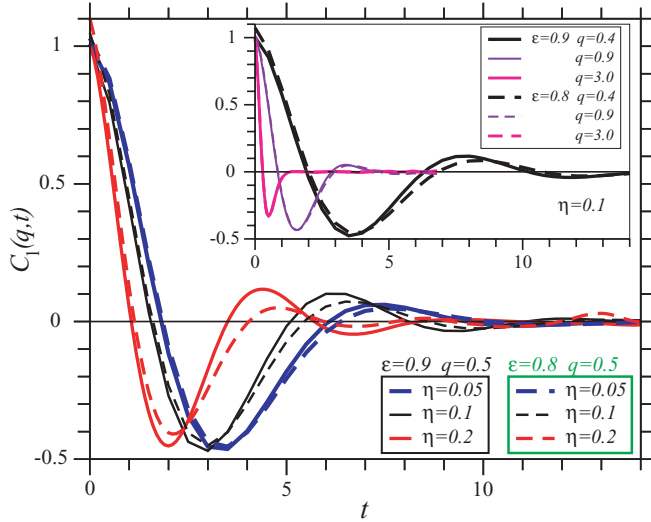


FIG. 8. (Color online) Longitudinal current correlation as a function of time for several densities. Inset: Variation with q .

speed of sound can be obtained from the maximum of $C_l(\mathbf{q}, \omega)$. The peak position ω_{\max} as a function of the wave number q is shown in Fig. 10. As shown in the inset, the peak position does not depend on ϵ . For small wave numbers a linear dispersion is observed (dashed lines in Fig. 10), while deviations from linear behavior for larger wave numbers are more pronounced for denser systems.

V. FLUCTUATING HYDRODYNAMICS

In this section we compute $S(q, \omega)$ from fluctuating hydrodynamics. Our presentation follows closely the work of van Noije *et al.* [19], except that we take care to conserve momentum at each instant in time, thereby avoiding a divergence of the static structure factor.

The hydrodynamic equations for the number density n and the flow velocity \mathbf{u} without driving are the same as for an elastic fluid. However, the equation for the temperature differs due to the energy dissipation in collisions and the energy input

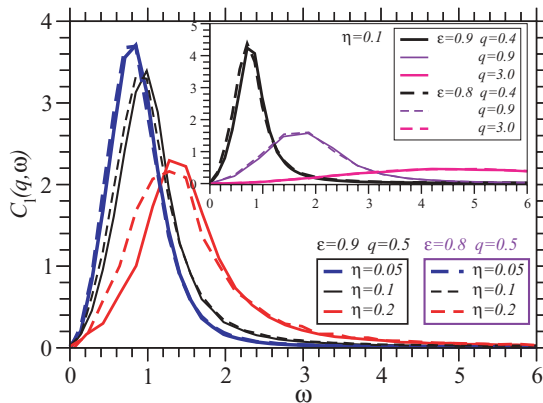


FIG. 9. (Color online) Longitudinal current correlation as a function of angular frequency.

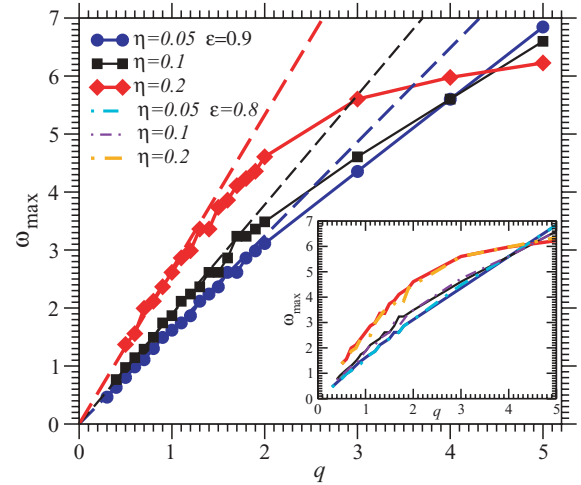


FIG. 10. (Color online) Position of the maximum ω_{\max} longitudinal current correlation $C_l(\mathbf{q}, \omega)$. Solid lines and filled symbols are for $\epsilon = 0.9$, and dashed lines indicate linear fits with slopes as listed in Table III. Inset: Comparison ω_{\max} for $\epsilon = 0.9$ (solid lines) and for $\epsilon = 0.8$ (dash-dotted lines).

due to driving:

$$\partial_t T = D_T \Delta T - \frac{2p}{dn} \nabla \mathbf{u} - \Gamma + m \xi_0^2 + \theta. \quad (13)$$

Here we present results in $d = 3$ dimensions. The energy dissipation due to collisions, Γ , is estimated as $\Gamma = 2T \nu_{\text{coll}} \frac{1-\epsilon^2}{2d}$ with collision frequency ν_{coll} . The input of kinetic energy due to driving is given by $m \xi_0^2$, p denotes the pressure, D_T the thermal diffusivity, and the noise θ will be specified below.

For a granular medium, Fourier's law should be generalized [29] to include a contribution to the heat current \mathbf{q} due to density gradients: $\mathbf{q} = -\kappa \nabla T + \mu \nabla n$. For elastic systems the transport coefficient μ has to vanish. For inelastic systems it has been estimated by various means [29–31]. It turns out that the coefficient μ is very small for driven systems. Garzó and Montanero [32] have computed it for the stochastic thermostat under consideration and compared it to the undriven system (see Fig. 3 in Ref. [32]). For the parameters under consideration, μ/κ is less than 13% and has been neglected. We have also ignored nonlinear terms involving the flow field because we consider only linear hydrodynamics.

In the stationary state the energy dissipation in collisions and the energy input due to driving balance on average:

$$\Gamma_0 = m \xi_0^2. \quad (14)$$

We expand in fluctuations around the stationary state: $n = n_0 + \delta n$, $T = T_0 + \delta T$, and $\Gamma = \Gamma_0 + \delta \Gamma$. The collision frequency should be proportional to the density, the pair correlation function at contact χ , and the thermal velocity, $\nu_{\text{coll}} \propto n \chi T^{1/2}$; hence linearization around the stationary state Γ_0 yields $\Gamma \sim \Gamma_0 (1 + \frac{\delta n}{n_0} + \frac{1}{\chi} \frac{d\chi}{dn} \delta n + \frac{3\delta T}{2T_0})$.

Following van Noije *et al.* [19], we consider a hydrodynamic description of a granular fluid based on conservation of particle number and momentum and the relaxation of temperature to its stationary value T_0 . The transverse momentum decouples so that we are left with three equations

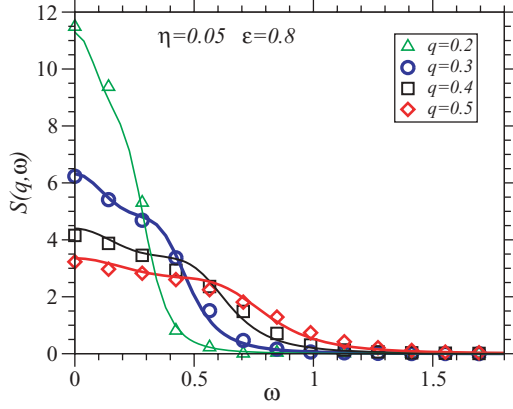


FIG. 11. (Color online) Dynamic structure factor $S(q, \omega)$ for $\eta = 0.05, \varepsilon = 0.8$, and $q = 0.2 - 0.5$. Symbols indicate simulation results obtained via Fourier transform of $F(q, t)$, and lines indicate fits with Eq. (33).

for the fluctuating density δn , the longitudinal flow velocity $u(\mathbf{q}, t) = \mathbf{q} \cdot \mathbf{u}/q$, and the fluctuating temperature δT :

$$\partial_t \delta n(\mathbf{q}, t) = -iqn_0 u(\mathbf{q}, t), \quad (15)$$

$$\begin{aligned} \partial_t u(\mathbf{q}, t) = & -\frac{iq}{mn_0} \left(\frac{\partial p}{\partial n} \delta n(\mathbf{q}, t) + \frac{\partial p}{\partial T} \delta T(\mathbf{q}, t) \right) \\ & -v_l q^2 u(\mathbf{q}, t) + \xi_1(\mathbf{q}, t), \end{aligned} \quad (16)$$

$$\begin{aligned} \partial_t \delta T(\mathbf{q}, t) = & -D_T q^2 \delta T(\mathbf{q}, t) - iq \frac{2p_0}{dn_0} u(\mathbf{q}, t) \\ & -\Gamma_0 \left(\frac{\delta n(\mathbf{q}, t)}{n_0} + \frac{1}{\chi} \frac{d\chi}{dn} \delta n(\mathbf{q}, t) + \frac{3}{2} \frac{\delta T(\mathbf{q}, t)}{T_0} \right) \\ & + \theta(\mathbf{q}, t), \end{aligned} \quad (17)$$

where $D_T = \frac{2\kappa}{dn_0}$ with the heat conductivity κ , and where v_l is the longitudinal viscosity. Fluctuating hydrodynamics for an elastic fluid ($\varepsilon = 1$) is based on internal noise, ξ_1^{in} and θ^{in} , consistent with the fluctuation-dissipation theorem. Here we consider a randomly driven system: the particles are kicked randomly, giving rise to external noise in the equation for the velocity as well as the temperature. The external contributions are

$$\xi_1^{\text{ex}}(\mathbf{r}, t) = \frac{1}{n_0} \sum_i \xi_{i1}(t) \delta(\mathbf{r} - \mathbf{r}_i) \quad (18)$$

and

$$\theta^{\text{ex}}(\mathbf{r}, t) = \frac{2m}{dn_0} \sum_i \mathbf{v}_i \cdot \xi_i(t) \delta[\mathbf{r} - \mathbf{r}_i(t)], \quad (19)$$

with variance

$$\langle \xi_1^{\text{ex}}(\mathbf{q}, t) \xi_1^{\text{ex}}(-\mathbf{q}, t') \rangle = V \frac{\xi_0^2}{n_0} \delta(t - t') (1 - \delta_{\mathbf{q}, 0}) \quad (20)$$

and

$$\langle \theta^{\text{ex}}(\mathbf{q}, t) \theta^{\text{ex}}(-\mathbf{q}, t') \rangle = V \frac{4mT_0}{dn_0} \xi_0^2 \delta(t - t'). \quad (21)$$

Here we have taken care of global momentum conservation, as realized by our driving mechanisms involving pairs of particles. Consequently, the driving force for the flow field vanishes at zero wave number. There is no global energy

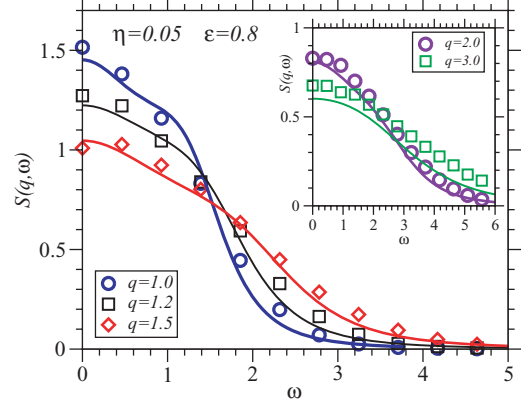


FIG. 12. (Color online) $S(q, \omega)$ for $\eta = 0.05, \varepsilon = 0.8$, and $q = 1.0 - 3.0$.

conservation and hence the noise variance is finite for 0 wave number. van Noije *et al.* [19] suggested including, in addition, internal noise, $\xi_1 = \xi_1^{\text{in}} + \xi_1^{\text{ex}}$ and $\theta = \theta^{\text{in}} + \theta^{\text{ex}}$, chosen according to the fluctuation-dissipation theorem. The variance of the total noise is then given by

$$\langle \xi_1(\mathbf{q}, t) \xi_1(-\mathbf{q}, t') \rangle = V \left(\frac{\xi_0^2}{n_0} + \frac{2v_l T_0 q^2}{mn_0} \right) \delta(t - t') (1 - \delta_{\mathbf{q}, 0}) \quad (22)$$

and

$$\langle \theta(\mathbf{q}, t) \theta(-\mathbf{q}, t') \rangle = 4V \left(\frac{mT_0 \xi_0^2}{dn_0} + \frac{2\kappa T_0^2 q^2}{d^2 n_0^2} \right) \delta(t - t'). \quad (23)$$

This choice seems rather intuitive and was suggested by van Noije *et al.* [19] on phenomenological grounds. It was later justified by Maynar *et al.* [33] for the transverse flow by deriving the fluctuating hydrodynamic equation from a Boltzmann-Langevin equation.

To complement the preceding equations, we need an expression for the pressure p in terms of the density and temperature. Since the driven granular gas is far from equilibrium, we cannot expect that a thermodynamic description including an equation of state should hold in general. Nevertheless, for small to

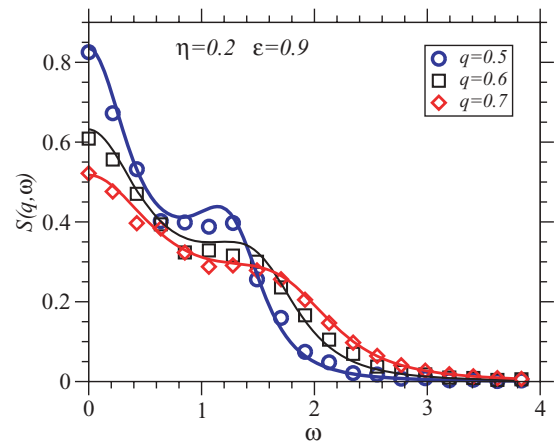


FIG. 13. (Color online) $S(q, \omega)$ for $\eta = 0.2, \varepsilon = 0.9$, and $q = 0.5 - 0.7$.

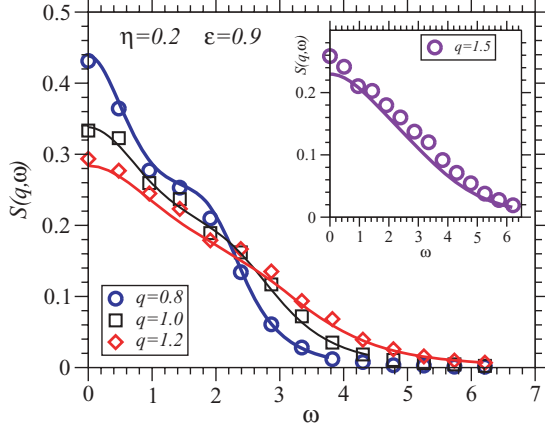


FIG. 14. (Color online) $S(q, \omega)$ for $\eta = 0.2, \epsilon = 0.9$, and $q = 0.8-1.5$.

moderate inelasticities an equation of state has been found empirically (Eq. (17.29) in Ref. [10]): $p \approx nT[1 + 2\eta\chi(1 + \epsilon)]$. We use the Carnahan-Starling approximation (for $d = 3$):

$$\chi = \frac{(1 - \eta/2)}{(1 - \eta)^3}. \quad (24)$$

This leaves us with two unknown parameters in the hydrodynamic description, namely, the longitudinal viscosity ν_l and the thermal diffusivity D_T .

The linearized equations can be solved for the frequency- and wave-number-dependent correlation functions, $S(q, \omega)$ and $C_l(q, \omega) = \frac{\omega^2}{q^2} S(q, \omega)$. Of particular interest is the pole structure in the complex ω plane, describing damped sound modes and the decay of temperature fluctuations. The latter can be either diffusive or at a finite relaxation rate, depending on the wave number q . For $D_T q^2 \ll \frac{3\Gamma_0}{2T_0}$, the thermal diffusivity can be ignored and we have poles at

$$\omega_T = \pm i \frac{3\Gamma_0}{2T_0}, \quad (25)$$

$$\omega_s = \pm cq \pm i\gamma q^2. \quad (26)$$

The latter correspond to sound modes with sound velocity

$$c^2 = v_{\text{th}}^2 - \frac{2p_0}{3mn_0} \left(1 + \frac{n_0}{\chi} \frac{\partial \chi}{\partial n} \right), \quad (27)$$

TABLE I. Estimates for $q_c a$ using Eq. (32).

η	ϵ	$q_c a$
0.05	0.8	0.21
0.05	0.9	0.14
0.1	0.8	0.48
0.1	0.9	0.33
0.2	0.8	1.29
0.2	0.9	0.89

where $v_{\text{th}}^2 = \frac{1}{m} \left(\frac{\partial p}{\partial n} \right)_T$, and damping

$$2\gamma = \nu_l + \frac{4p_0 T_0}{3\Gamma_0 m n_0} \left(\frac{1}{3} \left[1 + \frac{n_0}{\chi} \frac{\partial \chi}{\partial n} \right] + \frac{p_0}{dT_0 n_0} \right). \quad (28)$$

In the opposite limit, $D_T q^2 \gg \frac{3\Gamma_0}{2T_0}$, we recover ordinary hydrodynamics of an elastic fluid. The sound speed is given by the adiabatic value,

$$c^2 = v_s^2 = v_{\text{th}}^2 + \frac{2p_0^2}{dmT_0 n_0^2}, \quad (29)$$

and the temperature decay is diffusive, $\omega_T = \pm i D_T q^2 \frac{v_{\text{th}}^2}{v_s^2}$.

In general, we expect to see a crossover when $D_T q_c^2 = \frac{3\Gamma_0}{2T_0}$. To estimate q_c , we use the Enskog values for the collision frequency in three dimensions and the thermal diffusivity:

$$\nu_{\text{coll}} = \omega_E = 4\pi \chi n_0 a^2 \sqrt{\frac{T_0}{\pi m}}, \quad (30)$$

$$D_T = \frac{75}{d(1 + \epsilon)(49 - 33\epsilon)n_0 a^2 \chi} \sqrt{\frac{T_0}{\pi m}}. \quad (31)$$

These yield, for the crossover wave number,

$$q_c^2 a^2 = \frac{6(1 - \epsilon^2)(1 + \epsilon)(49 - 33\epsilon)\chi^2 36\eta^2}{75\pi}. \quad (32)$$

Numerical values of estimated $q_c a$ for the simulated volume fractions η and inelasticities ϵ are listed in Table I.

For the case of $D_T q^2 \approx \frac{3\Gamma_0}{2T_0}$ it is necessary to use the more general solution for the dynamic structure factor,

$$S(q, \omega) = n_0 q^2 \left(\frac{[\omega^2 + (3\gamma_0 \omega_E + D_T q^2)^2] \left[\frac{\xi_0^2}{n_0} + \frac{2\nu_l T_0 q^2}{mn_0} \right] + q^2 \left(\frac{p_0}{mn_0 T_0} \right)^2 \left[\frac{4mT_0 \xi_0^2}{dn_0} + \frac{4D_T T_0 q^2}{dn_0} \right]}{|\det M|^2} \right), \quad (33)$$

where we have used $\nu_{\text{coll}} = \omega_E$, the abbreviation $\gamma_0 = \frac{1 - \epsilon^2}{2d}$, and where

$$|\det M|^2 = \left[-\omega^2 (3\gamma_0 \omega_E + D_T q^2 + \nu_l q^2) + q^2 \left(3\gamma_0 \omega_E v_{\text{th}}^2 - \frac{2p_0 \gamma_0 \omega_E}{mn_0} \left\{ 1 + \frac{n_0}{\chi} \frac{\partial \chi}{\partial n} \right\} + v_{\text{th}}^2 D_T q^2 \right) \right]^2 + \left[\omega^3 - \omega q^2 \left(3\nu_l \gamma_0 \omega_E + \nu_l D_T q^2 + v_{\text{th}}^2 + \frac{2p_0^2}{dmT_0 n_0^2} \right) \right]^2. \quad (34)$$

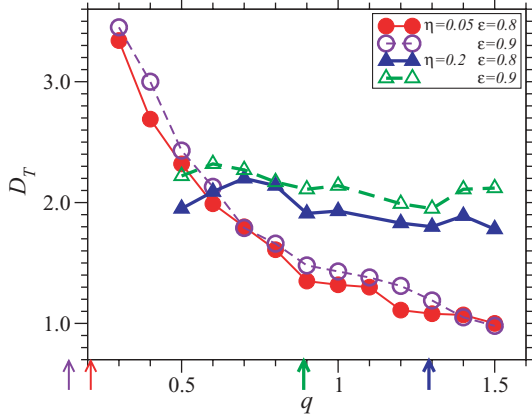


FIG. 15. (Color online) Thermal diffusivity $D_T(q)$ obtained via fits to $S(q, \omega)$ with Eq. (33). The arrows indicate the q_c values from Table I.

VI. COHERENT SCATTERING FUNCTION AND TRANSPORT COEFFICIENTS

According to the q_c estimates given in Table I, we see that our data are neither clearly in the hydrodynamic regime nor clearly in the inelastic regime, but in general the two relaxation terms in the equation for the temperature are comparable in magnitude. Hence, we fit the simulation results of the dynamic structure factor to the full expression for $S(q, \omega)$ as given in Eqs. (33) and (34). We allow for two fit parameters, D_T and ν_l , with all other parameters determined by the approximate equation of state. The best fits (solid line) are shown in Figs. 11–14, in comparison with the simulation data (symbols) for $S(q, \omega)$. We find excellent agreement not only for very small q , for which we would expect the best agreement with the hydrodynamic equations, but also for $q \lesssim 1.0$. Both features, the shoulder due to the sound wave as well as the damping, are quantitatively in agreement with Eqs. (33) and (34). Similarly, we find very good agreement for the $\eta = 0.1$ results.

The corresponding best fit-parameters are the transport coefficients D_T and ν_l , which are shown graphically in Figs. 15

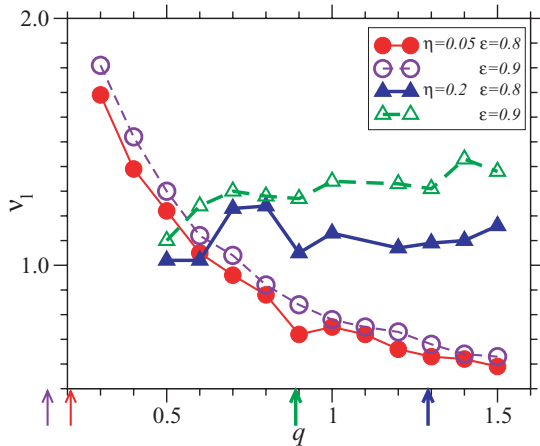


FIG. 16. (Color online) Longitudinal viscosity $\nu_l(q)$ obtained via fits to $S(q, \omega)$ with Eq. (33). Arrows indicate the q_c values from Table I.

and 16. The fits require q -dependent transport coefficients because we consider wave numbers outside the hydrodynamic regime. It is difficult to estimate the hydrodynamic regime, but we need at least $q < q_c$ (see Table II), corresponding to $D_T q^2 < \frac{3\Gamma_0}{2T_0}$. For $\eta = 0.2$, we are able to reach this regime and, indeed, find that D_T and ν_l are approximately independent of q . For $\eta = 0.05$, even the smallest q values are not in the hydrodynamic regime yet, and for $\eta = 0.1$ the smallest wave numbers are in the crossover regime. As far as temperature fluctuations are concerned, the diffusive regime is restricted to larger wave numbers, $D_T q^2 > \frac{3\Gamma_0}{2T_0}$, so that D_T can only be extracted from an intermediate range of q values, such that $q > q_c$ but q still small enough to ignore higher-order terms in q . Again, for $\eta = 0.2$ this seems possible, whereas for $\eta = 0.05$ our data are not sufficient.

Table II reports a quantitative comparison of the fit results for small q with the theoretical predictions for $D_T = \frac{2\kappa}{dn}$ and $\nu_l = \frac{1}{\rho} (2\eta_{\text{shear}} \frac{d-1}{d} + \zeta)$, where η_{shear} and ζ are the shear and bulk viscosity, respectively. For the comparison with

TABLE II. Comparison of theoretical predictions and fit results for D_T and ν_l .

	$\eta = 0.05$			
	$\varepsilon = 0.8$		$\varepsilon = 0.9$	
	D_T	ν_l	D_T	ν_l
Fit results				
$q = 0.2$	4.72	2.55	4.63	3.23
$q = 0.3$	3.34	1.69	3.45	1.81
$q = 0.4$	2.69	1.39	3.00	1.52
Brilliantov <i>et al.</i> [10]	3.19	2.26	3.54	2.25
Dufty <i>et al.</i> [34]	4.71	2.82	4.07	2.77
Garzó <i>et al.</i> [28]	5.62	2.78	5.06	2.67
Garzó <i>et al.</i> [32]	3.57	2.56	3.93	2.55
	$\eta = 0.1$			
	$\varepsilon = 0.8$		$\varepsilon = 0.9$	
	D_T	ν_l	D_T	ν_l
Fit results				
$q = 0.3$	2.23	1.20	2.67	1.70
$q = 0.4$	2.25	1.02	2.42	1.25
$q = 0.5$	2.15	1.07	2.33	1.20
Brilliantov <i>et al.</i> [10]	1.39	1.13	1.55	1.13
Dufty <i>et al.</i> [34]	2.67	1.69	2.42	1.71
Garzó <i>et al.</i> [28]	2.81	1.53	2.53	1.48
Garzó <i>et al.</i> [32]	1.78	1.42	1.97	1.42
	$\eta = 0.2$			
	$\varepsilon = 0.8$		$\varepsilon = 0.9$	
	D_T	ν_l	D_T	ν_l
Fit results				
$q = 0.5$	1.95	1.02	2.22	1.10
$q = 0.6$	2.09	1.02	2.32	1.24
$q = 0.7$	2.20	1.23	2.27	1.30
Brilliantov <i>et al.</i> [10]	0.52	0.83	0.57	0.85
Dufty <i>et al.</i> [34]	2.03	1.63	2.01	1.72
Garzó <i>et al.</i> [28]	1.40	1.15	1.26	1.15
Garzó <i>et al.</i> [32]	0.89	1.10	0.98	1.12

TABLE III. Speed of sound c determined via the slope of the simulation results for $\omega_{\max}(q)$ (see Fig. 10) compared with the predicted values of Eq. (27) in the case of $D_T q^2 \ll \frac{3\Gamma_0}{2T_0}$ and with Eq. (29) in the case of $D_T q^2 \gg \frac{3\Gamma_0}{2T_0}$.

	Via $\omega_{\max}(q)$	$D_T q^2 \ll \frac{3\Gamma_0}{2T_0}$	$D_T q^2 \gg \frac{3\Gamma_0}{2T_0}$
$\epsilon = 0.8$			
$\eta = 0.05$	1.58	0.73	1.55
$\eta = 0.1$	1.81	0.90	1.87
$\eta = 0.2$	2.57	1.37	2.79
$\epsilon = 0.9$			
$\eta = 0.05$	1.62	0.74	1.56
$\eta = 0.1$	1.89	0.92	1.90
$\eta = 0.2$	2.66	1.40	2.86

Brilliantov *et al.*, we use Eqs. (20.13) and (20.30) of Ref. [10] for η_{shear} and κ , respectively, and ζ from Eq. (32) of Ref. [34]. For the predictions of Dufty *et al.*, we used Eqs. (29), (30), and (32) of Ref. [34], and for the predictions of Garzó *et al.* we used Eqs. (B1), (2.2), (3.8), (2.3), and (3.9) of Ref. [28]. All the preceding results refer to undriven systems, whereas in Ref. [32] the transport coefficients are computed for the stochastic thermostat under consideration. We used Eqs. (46), (47), and (B4) from Ref. [32] for comparison with our data. The transport coefficients computed from kinetic theory are all of the same order of magnitude but vary among themselves. Our results lie in the same range as their variations and none of the theoretical predictions is significantly superior to the others.

Finally, we compare the speed of sound as obtained from the maximum of the current correlation with the predictions from the hydrodynamic theory in either the inelastic regime [see Eq. (27)] or the diffusive regime [see Eq. (29)]. We find very good agreement (see Table III) of the simulation results with Eq. (29), implying $D_T q^2 \gg \frac{3\Gamma_0}{2T_0}$ and adiabatic sound propagation. However, one should keep in mind that our procedure to extract the sound velocity from the maximum of the current correlation yields only an estimate of the sound velocity.

VII. CONCLUSIONS AND OUTLOOK

We have investigated a homogeneously driven granular fluid of hard spheres at intermediate volume fractions $0.05 \leq \eta \leq 0.4$ and for constant normal restitution coefficients $0.8 \leq \epsilon \leq 1.0$. Using event-driven simulations we have determined time-delayed correlation functions in the stationary state.

We find that the incoherent intermediate scattering function follows time-density superposition and that it is well approximated by the Gaussian $F_{\text{incoh}}(\mathbf{q}, t) = e^{-\frac{\eta^2}{6} \langle \Delta r^2(t) \rangle}$, where $\langle \Delta r^2(t) \rangle$ is the mean square displacement. The decay time of $F_{\text{incoh}}(\mathbf{q}, t)$ increases rapidly with increasing η , giving rise to a corresponding decrease in the diffusion constant. This precursor of a glass transition, which occurs at significantly larger η , is thus present not only in the elastic fluid but also in the inelastic case, consistent with previous results at higher densities [14,22,27].

We also determine the coherent intermediate scattering function $F(q, t)$, the longitudinal current correlation function $C_1(q, t)$, and their Fourier transforms $S(q, \omega)$ and $C_1(q, \omega)$. Because we are interested in the long-term dynamics, we have simulated comparatively small systems of $N = 10,000$ particles and averaged over 100 independent simulation runs. We observe sound waves in the form of oscillations in $F(q, t)$ and estimate the sound velocity from the peak of $C_1(q, t)$. For a quantitative comparison with the predictions of generalized fluctuating hydrodynamics, we use the linear hydrodynamic equations of Noije *et al.* [19] and fit the solutions thereof to the simulation results for $S(q, \omega)$. Depending on the wave number and inelasticity, the temperature fluctuations are predicted to be governed by inelastic collisions or diffusion [19,35]. Our results are consistent with being in the “standard regime” [19], in which the speed of sound is the same as for elastic particles (see Table III) and the damping of the sound wave depends on inelasticity. The most accurate fits were obtained assuming generalized hydrodynamic equations that account for both temperature diffusion as well as dissipation due to inelastic collisions [Eq. (33)]. The resulting transport coefficients D , D_T , and v_1 compare well with the predictions of Dufty *et al.* [34] and Garzó *et al.* [28].

We conclude that the time-delayed correlations of a fluid of inelastically colliding particles are well described by generalized hydrodynamics. It would be interesting to extend our study in several directions. First, one would like to see still smaller q , requiring significantly larger systems (and yet also many independent runs for sufficient statistics). Second, it would be interesting to go to higher density and study sound propagation as the glass transition is approached. Finally, time- or frequency-dependent response functions are largely unexplored.

ACKNOWLEDGMENTS

K.V.L. thanks the Institute of Theoretical Physics, University of Göttingen, for financial support and hospitality. The authors thank Till Kranz for many interesting discussions.

[1] C. S. Campbell, *Annu. Rev. Fluid Mech.* **22**, 57 (1990).
 [2] J. J. Brey, J. W. Dufty, C. S. Kim, and A. Santos, *Phys. Rev. E* **58**, 4638 (1998).
 [3] N. Sela and I. Goldhirsch, *J. Fluid Mech.* **361**, 41 (1998).
 [4] I. Goldhirsch, *Annu. Rev. Fluid Mech.* **35**, 267 (2003).
 [5] M.-L. Tan and I. Goldhirsch, *Phys. Rev. Lett.* **81**, 3022 (1998).
 [6] I. Goldhirsch and G. Zanetti, *Phys. Rev. Lett.* **70**, 1619 (1993).

[7] O. Herbst, P. Müller, M. Otto, and A. Zippelius, *Phys. Rev. E* **70**, 051313 (2004).
 [8] J. T. Jenkins and S. B. Savage, *J. Fluid Mech.* **130**, 187 (1983).
 [9] C. K. K. Lun, S. B. Savage, D. J. Jeffery, and N. Chepurnyi, *J. Fluid Mech.* **140**, 223 (1984).
 [10] N. V. Brilliantov and T. Pöschel, *Kinetic Theory of Granular Gases* (Oxford University Press, Oxford, 2004).

- [11] J. F. Lutsko, *Phys. Rev. Lett.* **86**, 3344 (2001).
- [12] A. Santos, *Phys. Rev. Lett.* **100**, 078003 (2008).
- [13] J. S. Olafsen and J. S. Urbach, *Phys. Rev. E* **60**, R2468 (1999).
- [14] F. V. Reyes and J. S. Urbach, *Phys. Rev. E* **78**, 051301 (2008).
- [15] J. J. Brey and M. J. Ruiz-Montero, *Phys. Rev. E* **81**, 021304 (2010).
- [16] M. Schröter, D. I. Goldman, and H. L. Swinney, *Phys. Rev. E* **71**, 030301(R) (2005).
- [17] A. R. Abate and D. J. Durian, *Phys. Rev. E* **74**, 031308 (2006).
- [18] T. P. C. van Noije, M. H. Ernst, and R. Brito, *Phys. Rev. E* **57**, R4891 (1998).
- [19] T. P. C. van Noije, M. H. Ernst, E. Trizac, and I. Pagonabarraga, *Phys. Rev. E* **59**, 4326 (1999).
- [20] I. Pagonabarraga, E. Trizac, T. P. C. van Noije, and M. H. Ernst, *Phys. Rev. E* **65**, 011303 (2001).
- [21] A. Fiege, T. Aspelmeier, and A. Zippelius, *Phys. Rev. Lett.* **102**, 098001 (2009).
- [22] W. T. Kranz, M. Sperl, and A. Zippelius, *Phys. Rev. Lett.* **104**, 225701 (2010).
- [23] A. Panaitescu and A. Kudrolli, e-print [arXiv:1001.0625v1](https://arxiv.org/abs/1001.0625v1) [cond-mat.mtrl-sci].
- [24] D. R. M. Williams and F. C. MacKintosh, *Phys. Rev. E* **54**, R9 (1996).
- [25] P. Espanol and P. Warren, *Europhys. Lett.* **30**, 191 (1995).
- [26] B. D. Lubachevsky, *J. Comput. Phys.* **94**, 255 (1991).
- [27] P. M. Reis, R. A. Ingale, and M. D. Shattuck, *Phys. Rev. Lett.* **98**, 188301 (2007).
- [28] V. Garzó, A. Santos, and J. M. Montanero, *Physica A* **376**, 94 (2007).
- [29] J. T. Jenkins and M. W. Richman, *Phys. Fluids* **28**, 3485 (1985).
- [30] R. Soto, M. Mareschal, and D. Risso, *Phys. Rev. Lett.* **83**, 5003 (1999).
- [31] O. Herbst, P. Müller, and A. Zippelius, *Phys. Rev. E* **72**, 041303 (2005).
- [32] V. Garzó and J. M. Montanero, *Physica A* **313**, 336 (2002).
- [33] P. Maynar, M. I. G. de Soria, and E. Trizac, *Eur. Phys. J. Spec. Top.* **179**, 123 (2009).
- [34] J. W. Dufty, J. J. Brey, and A. Santos, *Physica A* **240**, 212 (1997).
- [35] S. McNamara, *Phys. Fluids A* **5**, 3056 (1993).